Nonlinear Dyn (2008) 54:3–12
DOI 10.1007/s11071-007-9238-x

ORIGINAL ARTICLE

Frequency locking in a forced Mathieu–van der Pol–Duffing system

Manoj Pandey · Richard H. Rand · Alan T. Zehnder

Received: 4 August 2006 / Accepted: 29 January 2007 / Published online: 22 February 2007

Abstract Optically actuated radio frequency microelectromechanical system (MEMS) devices are seen to self-oscillate or vibrate under illumination of sufficient strength (Aubin, Pandey, Zehnder, Rand, Craighead, Zalalutdinov, Parpia (Appl. Phys. Lett. **83**, 3281–3283, 2003)). These oscillations can be frequency locked to a periodic forcing, applied through an inertial drive at the forcing frequency, or subharmonically via a parametric drive, hence providing tunability. In a previous work (Aubin, Zalalutdinov, Alan, Reichenbach, Rand, Zehnder, Parpia, Craighead (IEEE/ASME J. Micromech. Syst. **13**, 1018–1026, 2004)), this MEMS device was modeled by a three-dimensional system of coupled thermo-mechanical equations requiring experimental observations and careful finite element simulations to obtain the model parameters. The resulting system of equations is relatively computationally expensive to solve, which could impede its usage in a complex network of such resonators. In this paper, we present a simpler model that shows similar behavior to the MEMS device. We investigate the dynamics of a Mathieu–van der Pol–Duffing equation, which is forced both parametrically and nonparametrically. It is shown that the steady-state response can consist of either 1:1 frequency locking, or 2:1 subharmonic locking, or quasiperiodic motion. The system displays hysteresis when the forcing frequency is slowly varied. We use perturbations to obtain a slow flow, which is then studied using the bifurcation software package AUTO.

Keywords MEMS · Resonance · Parametric excitation · Quasiperiodic

M. Pandey · R. H. Rand (✉) · A. T. Zehnder
Department of Theoretical and Applied Mechanics, Cornell University, 207 Kimball Hall, Ithaca, NY 14853-1503, USA
e-mail: rhr2@cornell.edu

1 Introduction

Tunable limit cycle MEMS oscillators and resonators are becoming important components in radio frequency (RF) microsystems where they are used as electromechanical filters [3], amplifiers, and nonlinear mixers [4]. They also find use in different kinds of scanning probe microscopes [5, 6] as well as in biological and chemical sensors [7].

In previous works, MEMS devices consisting of a thin, planar, RF resonator [1, 2, 8, 9] were studied. These devices were shown to self-oscillate in the absence of external forcing, when illuminated by a DC laser of sufficient amplitude. This system can also be forced externally either parametrically, by modulating the incident laser, or nonparametrically, by using a piezo drive at the natural frequency of the device. In the presence of external forcing of sufficient strength and close enough in frequency to that of the unforced oscillation, the device will become frequency locked or get entrained by the forcer. A model was presented in [1, 2, 8, 9], which consisted of a third-order system

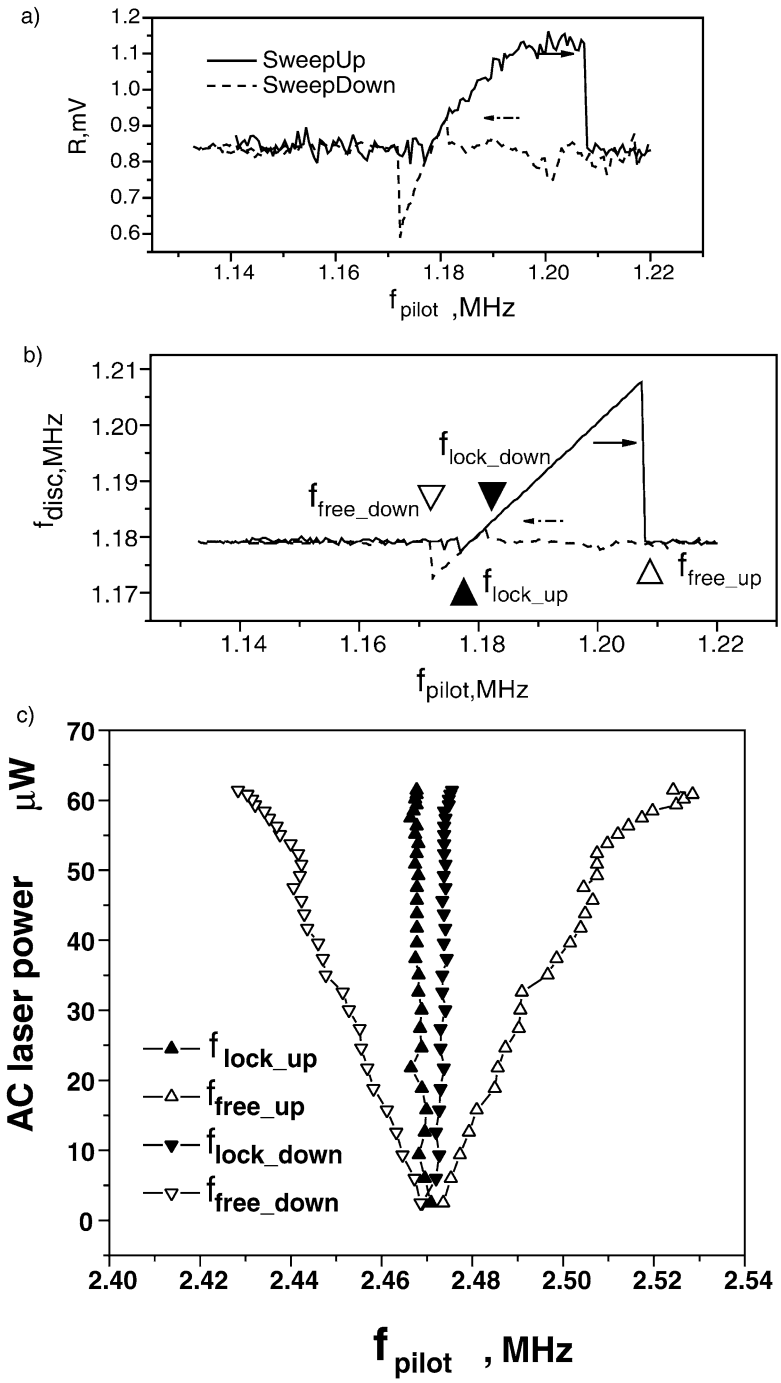

Fig. 1 Experimental results for entrainment in a CW laser driven, limit-cycle, disc resonator. (**a**) Amplitude response and (**b**) frequency response obtained when sweeping the frequency of inertial drive. (**c**) Entrainment region obtained when sweeping the modulation frequency of the incident laser about 2ω with no inertial drive. From [2]

of ODE's. Figure 1 shows the experimentally observed amplitude and frequency response close to entrainment. The limit cycle oscillation is entrained by the forcing, close to the natural frequency of the oscillator. Parametric variation of the entrainment region as a function of forcing amplitude is shown in Fig. 1c. The outer boundaries in Fig. 1c separate entrained regions from quasiperiodic response.

In this paper, a simpler model is studied, which still shows all the relevant phenomena seen in the disc resonator, namely, limit cycles, parametric excitation, and nonparametric excitation. The essential features

of the entrainment in a disc resonator can be listed as follows.

- For a DC laser of sufficient power, the disc resonator starts to self-oscillate at constant amplitude. The simplest canonical model which captures this behavior is a van der Pol oscillator [10]. It consists of an $-\epsilon\dot{x}(1-x^2)$ term added to a one-dimensional (1D) simple harmonic oscillator (SHO), which in the absence of forcing leads to a steady-state vibration called a limit cycle. For small values of ϵ, the limit cycle has frequency close to 1, which is the frequency of the unforced linear oscillator.
- The limit cycle in the system can be periodically forced either parametrically by modulating the laser, or nonparametrically by using a piezo drive. The Mathieu equation [10], which consists of adding a $\epsilon\alpha\cos(2\omega t)x$ term to a 1D SHO, can model parametric forcing of the system applied at twice the natural frequency of the resonator. This term in the absence of the van der Pol (vdP) term, renders the origin unstable when the parametric forcing frequency 2ω is close to twice the frequency of the unforced linear oscillator. Nonparametric forcing can be modeled by a term of form $F_0\sin\omega t$.
- When entrained, the system shows a backbone-shaped amplitude versus forcing frequency response. This kind of behavior is typical of the large amplitude response of structures and can be modeled by a Duffing's equation term [10], $\epsilon\beta x^3$, added to the SHO.

This paper concerns the following differential equation that may be thought of as a forced Mathieu–van der Pol–Duffing equation:

$$\ddot{x} + (1+\epsilon\alpha\ \cos(2\omega t+\phi))x - \epsilon\dot{x}(1-x^2) + \epsilon\beta x^3 = \epsilon F\ \cos\omega t \tag{1}$$

where $\epsilon\alpha$ is the magnitude of parametric forcing applied at frequency 2ω, and ϵF is the magnitude of nonparametric forcing applied at frequency ω while ϕ is the phase difference between the parametric and the nonparametric forcing. β is the coefficient of the cubic nonlinearity term and ϵ is a small parameter that will be used in the perturbation method. Equation (1) is combination of a vdP equation term [10], $-\epsilon\dot{x}(1-x^2)$, a Mathieu equation term [10], $\epsilon\alpha\cos(2\omega t)x$, and a Duffing's equation term, $(\epsilon\beta x^3)$, added to a forced SHO.

2 Numerical simulations

Numerical results and subsequent analysis are presented for two cases. To begin with, only nonparametric excitation is applied to the system. This corresponds to using $\alpha = 0$ in Equation (1). The numerical results in Fig. 2 show that away from the resonance i.e. for k_1 away from 1, the response consists of a quasiperiodic motion, which is a combination of contributions from the limit cycle and from the forcing. As the frequency is swept forward, the constant amplitude motion suddenly jumps onto a single frequency response, which increases in amplitude with a further increase in the

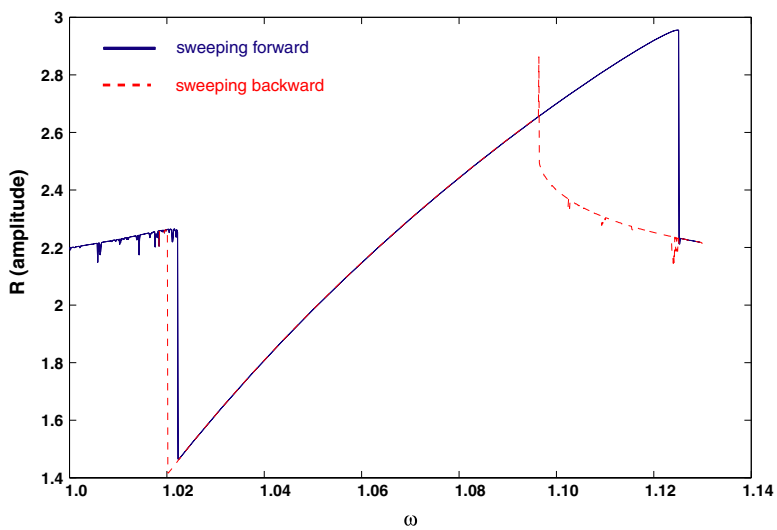

Fig. 2 Steady state solution obtained be numerical integration of Equation (1). $F = 3.0$, $\beta = 3.75$, $\alpha = 0.0$ and $\epsilon = 0.1$

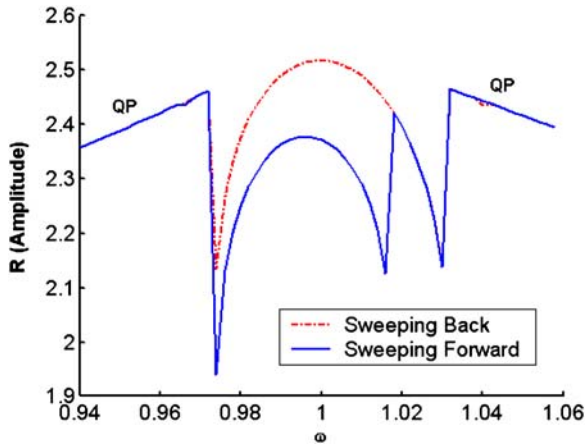

Fig. 3 Results of numerical integration of Equation (1) for parameters $\epsilon = 0.1$, $\alpha = 1$, $\beta = 0$, $F = 0.3$ and $\phi = 0$. Response amplitude R is plotted against forcing frequency ω. Quasiperiodic behavior (QP) is observed in the regions located approximately at $\omega < 0.97$ and $\omega > 1.03$. Periodic behavior at the forcing frequency is observed in the rest of the plot with hysteresis as shown

forcing frequency. Beyond a certain forcing frequency, the motion jumps back to the lower amplitude limit cycle response. Hysteresis is seen when the frequency is swept back. This response is similar to the experimentally obtained response for the disk resonator.

Next, the parametric forcing is also switched on and response amplitude as a function of forcing frequency ω for a case with parameters $\epsilon = 0.1$, $\alpha = 1$, $F = 0.3$, $\beta = 0.0$, and $\phi = 0$ is shown in Fig. 3. The cubic nonlinearity (β) is not considered here to simplify the subsequent analysis. Quasiperiodic behavior (QP) is observed in the regions located approximately at $\omega < 0.97$ and $\omega > 1.03$. Periodic behavior at the forcing frequency is observed in the rest of the plot, corresponding to entrainment. As we sweep the frequency forward, inside the entrained region, the amplitude jumps to a higher value at a frequency $\omega \approx 1.015$. No comparable jump is seen when the frequency is swept backward, indicating hysteresis.

We note that the parameters used in Figs. 2 and 3 have been chosen to illustrate the hysteresis exhibited by the model system of Equation (1) and are not obtained from the MEMS device referred to in Fig. 1.

3 Perturbation scheme

We use the two variable expansion method (also known as the method of multiple scales) to obtain an approximate analytic solution for Equation (1). The idea of this method is to replace time t by two time scales, $\xi = \omega t$, called stretched time, and $\eta = \epsilon t$, called slow time. The forcing frequency ω is expanded around the natural frequency of the oscillator ($\omega = 1$), i.e.,

$$\omega = 1 + k_1\epsilon + O(\epsilon^2) \tag{2}$$

where k_1 is a detuning parameter at order ϵ. Next, x is expanded in a power series in ϵ:

$$x = x_0(\xi, \eta) + \epsilon x_1(\xi, \eta) + O(\epsilon^2). \tag{3}$$

Substituting Equations (2) and (3) into (1) and collecting terms gives:

$$x_{0\xi\xi} + x_0 = 0 \tag{4}$$

$$x_{1\xi\xi} + x_1 = -2k_1 x_{0\xi\xi} - 2x_{0\xi\eta} + \left(1 - x_0^2\right)x_{0\xi} - \alpha x_0 \cos(2\xi + \phi) - \beta x_0^3 + F\cos\xi. \tag{5}$$

We take the solution to Equation (4) in the form:

$$x_0(\xi, \eta) = A(\eta)\ \cos\xi + B(\eta)\ \sin\xi \tag{6}$$

Substitution of Equation (6) into (5) and removal of secular terms gives the following slow flow, where primes represent differentiation with respect to η:

$$A' = -Bk_1 + \frac{A}{2} - \frac{A}{8}(A^2 + B^2) - \frac{\alpha}{4}(A\sin\phi + B\cos\phi) + \frac{3\beta B}{8}(B^2 + A^2). \tag{7}$$

$$B' = Ak_1 + \frac{B}{2} - \frac{B}{8}(A^2 + B^2) - \frac{\alpha}{4}(A\cos\phi - B\sin\phi) - \frac{3\beta A}{8}(B^2 + A^2) + \frac{F}{2} \tag{8}$$

From Equation (6), we see that a fixed point in the slow flow corresponds to a periodic motion in the original equation, while a limit cycle in the slow flow

corresponds to a quasiperiodic motion in the original equation.

4 Perturbation results for nonparametric excitation

In this section, results are shown for the case when parametric forcing is switched off ($\alpha = 0$). The slow flow in this case reduces to

$$A' = -Bk_1 + \frac{A}{2} - \frac{A}{8}(A^2 + B^2) + \frac{3\beta B}{8}(B^2 + A^2) \tag{9}$$

$$B' = Ak_1 + \frac{B}{2} - \frac{B}{8}(A^2 + B^2) - \frac{3\beta A}{8}(B^2 + A^2) + \frac{F}{2} \tag{10}$$

Figure 4 shows the results of applying the continuation software AUTO [11] to Equations (9) and (10). The amplitude of the fixed point and the radius of the limit cycle are displayed as functions of forcing frequency. The phase plane plots associated with different regions are also shown.

As expected, away from the resonance, a limit cycle is seen to coexist with an unstable fixed point, which is close to zero. As the forcing frequency gets closer to the resonant frequency, the unstable fixed point increases in amplitude and undergoes supercritical Hopf bifurcation at point 1, becoming a stable fixed point in the process. The stable limit cycle disappears at this point, and the motion jumps onto the stable fixed point. The system is now entrained by the forcing, and it follows the resonance curve of the Duffing oscillator, increasing in amplitude all the while until point 3. A saddle point arises at point 4 from a saddle node bifurcation and has amplitude close to but lower than the mentioned stable fixed point of the resonance curve. The stable fixed point disappears next in a saddle node bifurcation with the saddle point, close to the resonance curve at point 3. The motion then jumps back to the limit cycle with further increase in forcing frequency. When the frequency is swept back, it is clear that the point at which the limit cycle would be entrained must be different from the point at which the resonance curve disappears. The entrainment in this case is achieved when the limit cycle undergoes a fold by coalescing with an unstable limit cycle which is born in a homoclinic bifurcation near point 4 and, hence, the motion jumps back to the stable fixed point at 4. The system then follows the resonance curve until the Hopf bifurcation point 1. Hysteresis is seen in the dependence of the entrainment region on the direction of sweep.

5 Perturbation results for parametric excitation

In this section, we study the effect of switching on the parametric forcing ($\alpha \neq 0$). We set $\beta = 0$ (no Duffing x^3 term) to simplify the analysis. Thus, (7) and (8) reduce to following

$$A' = -Bk_1 + \frac{A}{2} - \frac{A}{8}(A^2 + B^2) - \frac{\alpha}{4}(A \sin\phi + B\cos\phi) \tag{11}$$

$$B' = Ak_1 + \frac{B}{2} - \frac{B}{8}(A^2 + B^2) - \frac{\alpha}{4}(A\cos\phi - B\sin\phi) + \frac{F}{2} \tag{12}$$

5.1 Invariances of the slow flow

The slow flow (11) and (12) contains four parameters: detuning k_1, parametric forcing amplitude α, nonparametric forcing amplitude F, and the phase difference ϕ. We shall be interested in understanding how the phase portrait of the slow flow is determined by these parameters. However, before discussing this, we note that Equations (11) and (12) exhibit some invariances, which permit useful conclusions to be drawn. For example, (11) and (12) remain unchanged when A, B, and F are replaced respectively by $-A$, $-B$, and $-F$. Since such a change does not alter the nature of the phase portrait, we see that *we may consider* $F \geq 0$ *without loss of generality*.

In addition, we see that Equations (11) and (12) remain unchanged when A, k_1, α, and ϕ are replaced respectively by $-A$, $-k_1$, $-\alpha$, and $-\phi$. Since changing the sign of A does not alter the nature of the phase portrait, we see that *we may consider* $\alpha \geq 0$ *without loss of generality* since negative α just reverses the k_1 and ϕ axes in the $k_1 - F - \phi$ bifurcation diagram, which leaves it essentially unchanged.

By the same reasoning, we may consider $\phi \geq 0$ without loss of generality, since replacing ϕ by $-\phi$ leaves the $k_1 - F - \alpha$ bifurcation diagram essentially

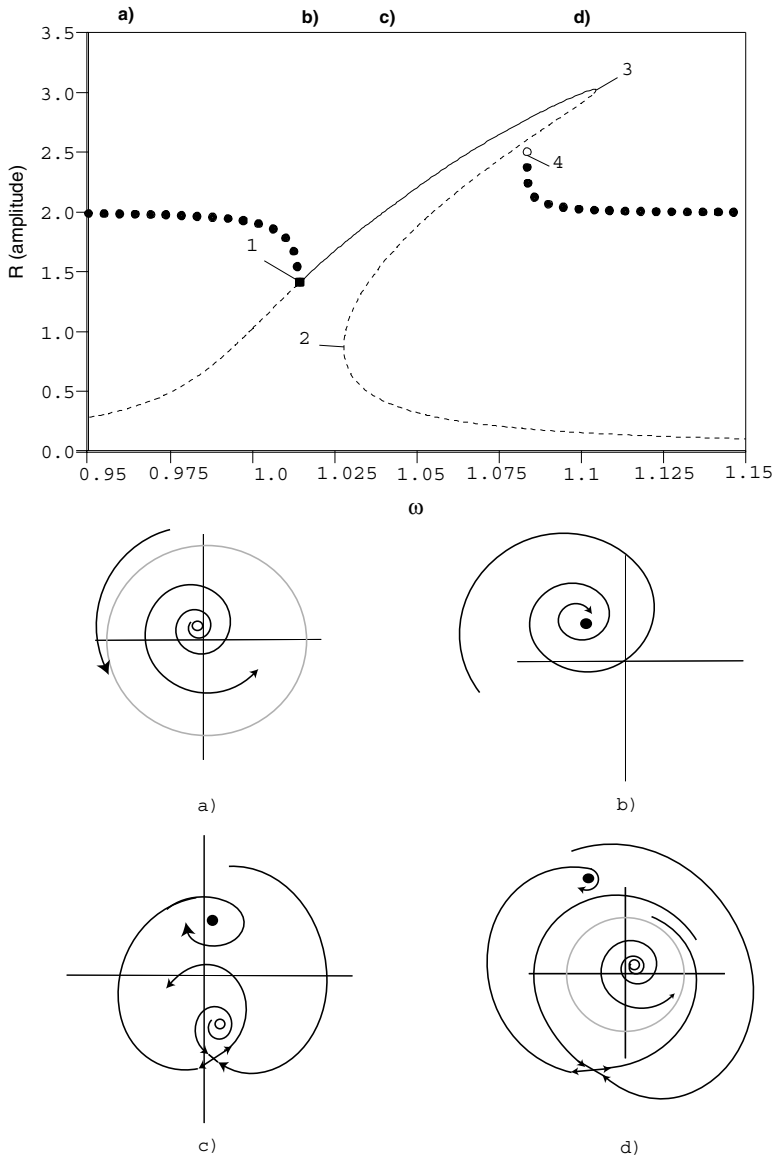

Fig. 4 Perturbation results obtained by applying the continuation software AUTO to Equations (9) and (10). $F = 3.0$, $\beta = 3.75$ and $\epsilon = 0.1$. The darkly *dotted curves* signify limit cycles in the slow flow, which correspond to quasiperiodic motions in the original equation

unchanged. However, since Equations (11) and (12) are 2π-periodic in ϕ, we may equally well choose ϕ to lie in any interval of length π. *Hence, we may consider* $-\frac{\pi}{2} < \phi < \frac{\pi}{2}$ *without loss of generality*.

5.2 Parametric study

Figure 5 shows the results of the AUTO [11] analysis for $\alpha = 1$ and $\phi = 0$, where k_1 and F are varied. Region A contains five slow flow equilibria, consisting of two sinks, two saddles, and one source, i.e., only two are stable. These stable equilibria correspond to frequency locked periodic motions in Equation (1). The presence of two such steady states signals the possibility of hysteresis. This same (stable) steady state occurs in region D that lies above region A in Fig. 5. The difference between these two regions is that D contains only three slow flow equilibria, namely, two sinks and a saddle. As we cross the curve separating A and D, two of the saddles in A merge with the source in region A in a pitchfork bifurcation, leaving a single saddle in their place.

We next consider regions E and B that lie to the left and right of region A, respectively, as shown in Fig. 5. The slow flow phase portrait for points in these two regions are qualitatively the same, consisting of three slow flow equilibria, namely, a source, a saddle, and

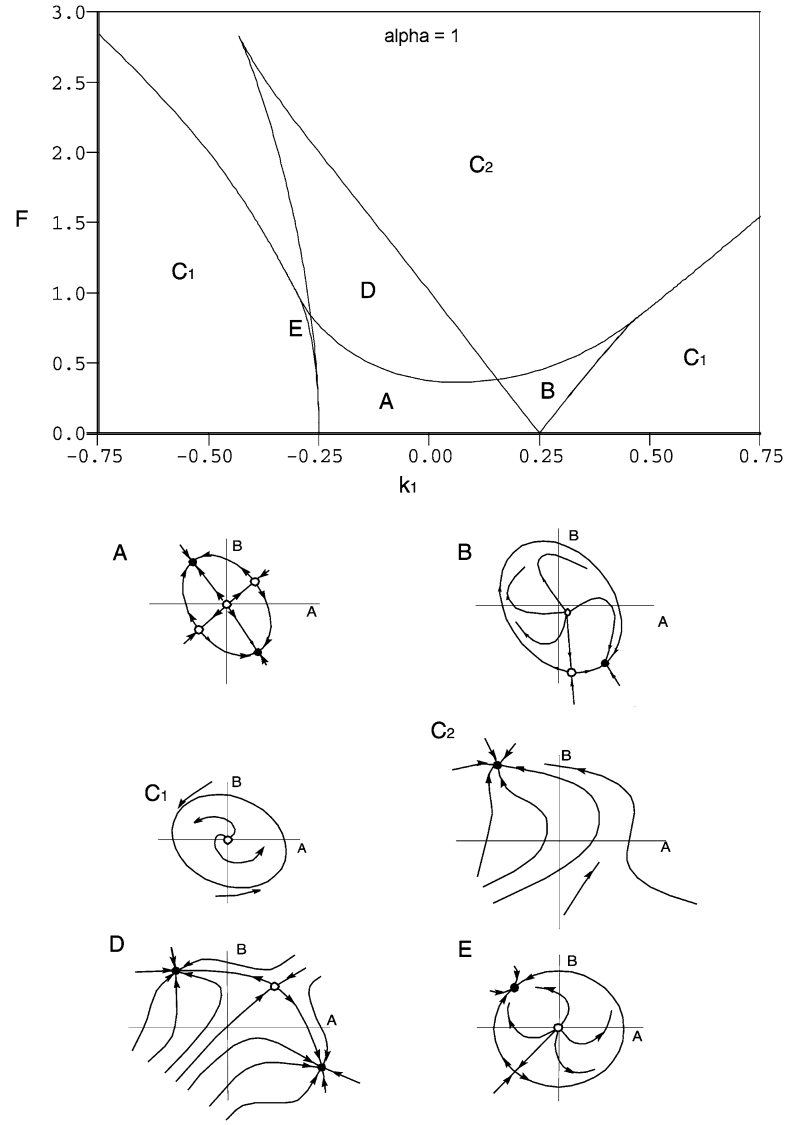

Fig. 5 Behavior of the slow flow (11) and (12). Bifurcation curves (obtained using AUTO) and sketches of corresponding slow flow phase portraits are displayed for $\alpha = 1$ and $\phi = 0$

a sink. Only one of these slow flow equilibria is stable and corresponds to a periodic motion at the forcing frequency in Equation (1). This same (stable) steady state occurs in region C_2 that lies above region D in Fig. 5. The difference between region C_2 and regions E and B is that C_2 contains just one slow flow equilibrium point, namely, a sink. As we cross the curve separating C_2 from one of the regions E, D, or B below it (each of which contains three slow flow equilibria), a saddle-node bifurcation occurs leaving a single sink in region C_2.

We have now discussed all regions in Fig. 5 except for regions C_1 that lie in the lower left and right portions of Fig. 5. Regions C_1 contain a single unstable slow flow equilibrium point, namely, a source. However, unlike the other regions in Fig. 5, regions C_1 also contain a stable slow flow limit cycle. This motion corresponds to a stable quasiperiodic motion in Equation (1). Hopf bifurcations occur along the curves separating regions C_1 and C_2.

We offer the following summary of predicted (stable) steady state behavior of Equation (1): In regions A and D, we have 2 distinct stable periodic motions; in regions E, C_2, and B, we have a single stable periodic motion; and in regions C_1, we have a stable quasiperiodic motion.

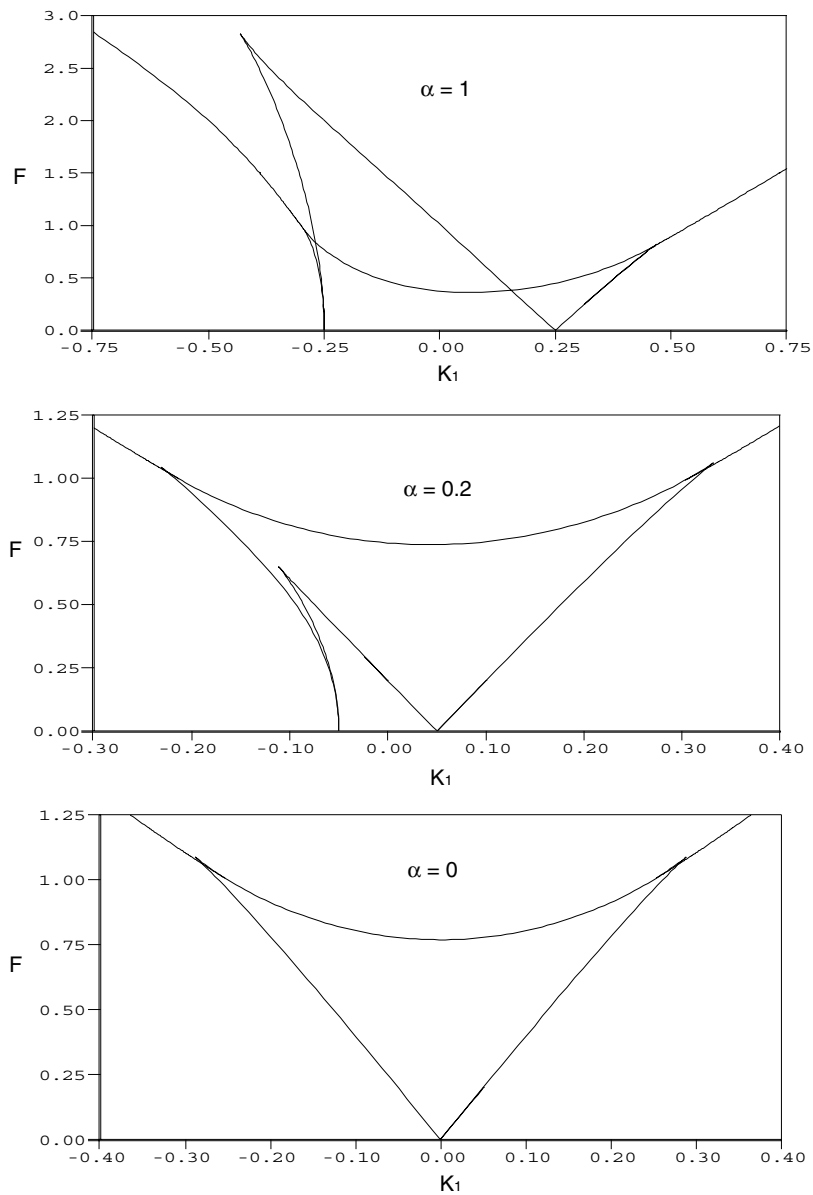

Fig. 6 Bifurcation curves (obtained using AUTO) for slow flow (11) and (12) for $\alpha = 1$, 0.2 and 0. $\phi = 0$ in all the cases. The figure at top is the same as that in Fig. 5

The discussion thus far has fixed α at unity (Fig. 5). Next, we look at the effect of changing α; see Fig. 6). We see that the width of the region corresponding to two distinct steady state periodic motions (regions A and D) decreases as we decrease α. In addition, the regions B and E become more symmetrical. For $\alpha = 0.2$, we see that the region D has disappeared and the regions E and B have merged to give just one region. At $\alpha = 0$, the region with two stable steady states has disappeared. This case corresponds to nonparametric periodic forcing of a van der Pol oscillator and has been discussed in [12].

Thus, the presence of the regions A and D that contain two stable periodic motions may be associated with the parameter α. Since α is the coefficient of the parametric excitation term, which has frequency 2ω, we may associate these regions with 2:1 subharmonic response. This is in contrast to regions E, B, and C_2, which may be associated with 1:1 frequency locking.

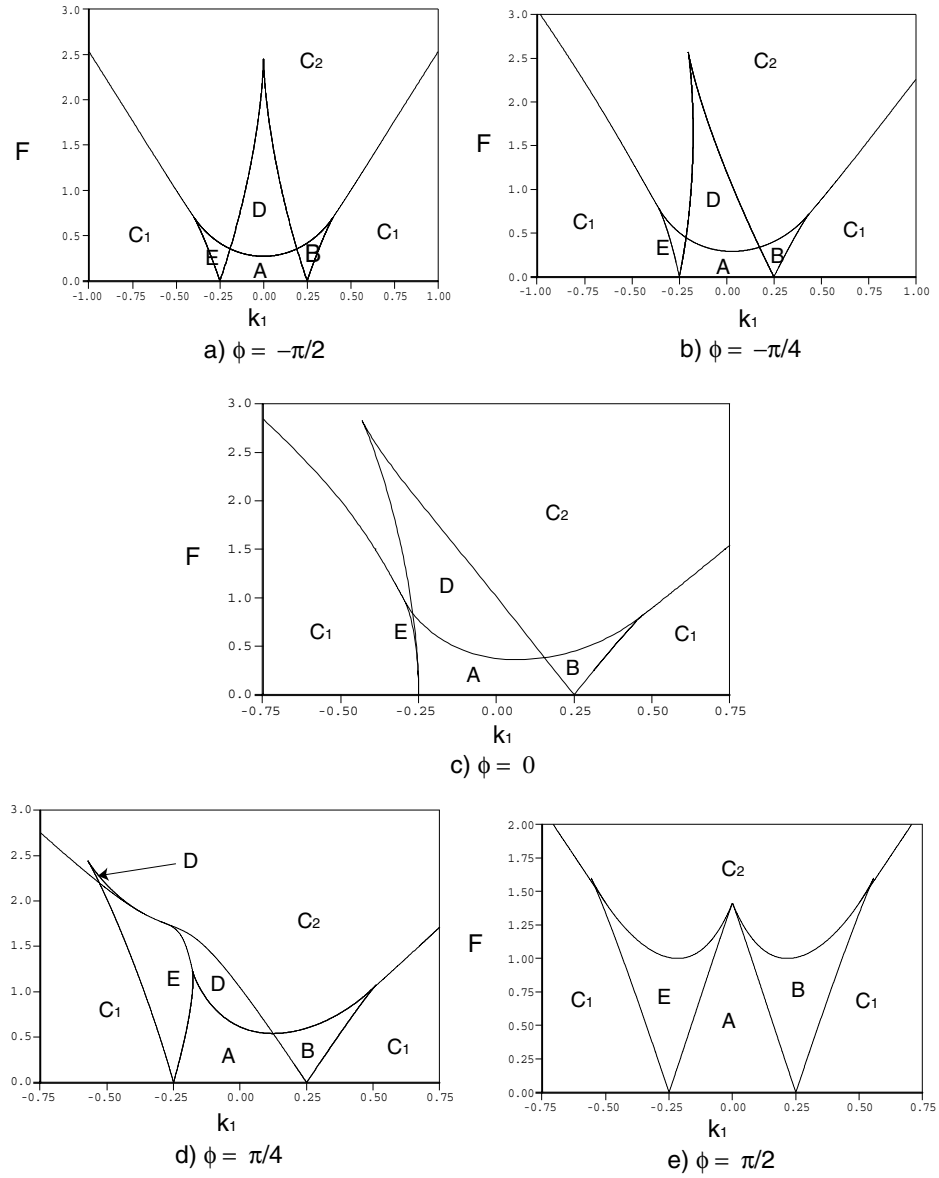

Fig. 7 Bifurcation curves (obtained using AUTO) for slow flow (11) and (12) for $\phi = \frac{-\pi}{2}, \frac{-\pi}{4}, 0, \frac{\pi}{4}$ and $\frac{\pi}{2}$. $\alpha = 1$ in all the cases

The dependence of the bifurcation curves of Fig. 5 on ϕ is displayed in Fig. 7. The diagram is seen to be symmetric about $k_1 = 0$ for $\phi = \frac{\pi}{2}$ and $\phi = -\frac{\pi}{2}$. As long as the nonparametric forcing leads the parametric forcing (i.e., $-\frac{\pi}{2} < \phi < 0$), decreasing phase magnitude $|\phi|$ bends the region of 2:1 entrainment (regions A and D) to the left. As a result, region E becomes very small for $\phi = 0$. On the other hand, when the parametric forcing leads the nonparametric forcing (i.e., $0 < \phi < \frac{\pi}{2}$), increasing ϕ causes region E to increase in size at the expense of region D, until at $\phi = \frac{\pi}{2}$, region D completely disappears, and the region E is the same size as B. For values of ϕ in the range $[\frac{\pi}{2}, \frac{3\pi}{2}]$, the $k_1 - F$ bifurcation diagram is essentially the same as shown in Fig. 7 , as discussed earlier in the section on invariances of the slow flow.

6 Conclusion

In this paper, we have presented the analysis of entrainment behavior in simplified canonical models of forced

limit cycle oscillators. We showed that these models captured many details of the steady-state response of a MEMS disk oscillator, which had been studied in previous works. The models studied in this paper are substantially simpler than the third-order system of ODE's, which was previously used to model the MEMS device, and as a result, the models presented here are expected to be more useful in studies of networks of coupled disk oscillators.

In the case of nonparametric excitation, we treated a forced van der Pol-Duffing system, Equation (1) with $\alpha = 0$, which exhibited a limit cycle being entrained by a periodic forcing function when the forcing frequency is close to the natural frequency of the system. In particular, Fig. 4 shows how the classic amplitude–frequency relation of the forced Duffing equation becomes modified when the unforced system exhibits a limit cycle.

In the case of parametric excitation, we treated a forced Mathieu–van der Pol system, Equation (1) with $\beta = 0$, which exhibited either 2:1 subharmonic motion or 1:1 periodic motion, or quasiperiodic motion, depending on the forcing frequency and the forcing amplitudes, both parametric and nonparametric. The findings may be summarized briefly in words (for fixed α) by stating that parametric excitation is most important when ω is close to the unforced frequency of the oscillator (here taken as unity), or, in other words, when the detuning k_1 is close to zero, and when F is small. Nonparametric forcing takes over when $|k_1|$ is a little larger or when F is larger. Quasiperiodic behavior occurs when $|k_1|$ becomes sufficiently large for given F.

Finally, we note that the hysteresis observed using slowly varying forcing frequency, in both experiments (Fig. 1) and in numerical simulations (Figs. 2 and 3), is explained by changes in the nature of the steady state due to bifurcations in the slow flow equilibria. For example, the jump upwards in Fig. 3 is due to passage from region A to region B in Fig. 5, in the process of which a saddle-node bifurcation occurs and a stable periodic motion disappears.

Acknowledgement This work was partially supported under the CMS NSF grant CMS-0600174 "Nonlinear Dynamics of Coupled MEMS Oscillators".

References

1. Aubin, K.L., Pandey, M., Zehnder, A.T., Rand, R.H., Craighead, H.G., Zalalutdinov, M., Parpia, J.M.: Frequency entrainment for micromechanical oscillator. Appl. Phys. Lett. **83**, 3281–3283 (2003)
2. Aubin, K., Zalalutdinov, M., Alan, T., Reichenbach, R., Rand, R., Zehnder, A., Parpia, J., Craighead, H.: Limit cycle oscillations in CW laser driven NEMS. IEEE/ASME J. Micromech. Syst. **13**, 1018–1026 (2004)
3. Wong, A.-C., Nguyen, C.T.-C., Ding, H.: RF MEMS for wireless applications. In: IEEE International Solid-State Circuits Conference, Vol. 448, p. 78 (1999)
4. Aubin, K.L., Zalautdinov, M., Reichenbach, R.B., Houston, B., Zehnder, A.T., Parpia, J.M., Craighead, H.G.: Laser annealing for high-q MEMS resonators. Proc. SPIE **5116**, 531–535 (2003)
5. Scherer, V., Hartmann, U., Goldade, A., Bhushan, B., Reinstadtler, M., Rabe, U., Arnold, W.: On the nanoscale measurement of friction using atomic-force microscope cantilever torsional resonances. Appl. Phys. Lett. **82**, 2604–2606 (2003)
6. Bruland, K.J., Rugar, D., Zuger, O., Hoen, S., Sidles, J.A., Garbini, J.L., Yannoni, C.S.: Magnetic resonance force microscopy. Rev. Mod. Phys. **67**, 249 (1995)
7. Sarid, D.: Scanning Force Microscopy with Applications to Electric, Magnetic and Atomic Forces. Oxford University Press, New York (1994)
8. Pandey, M., Aubin, K., Zalalutdinov, M., Zehnder, A., Rand, R.: Analysis of frequency locking in optically driven MEMS resonators. IEEE J. Microelectromech. Syst. **15**, 1546–1554 (2006)
9. Pandey, M., Rand, R., Zehnder, A.: Perturbation analysis of entrainment in a micromechanical limit cycle oscillator. Commun. Nonlinear Sci. Numer. Simulation, doi: 10.1016/j.cnsns.2006.01.017 (in press)
10. Nayfeh, A.H., Mook, D.T.: Nonlinear Oscillations. Wiley-Interscience, New York (1979)
11. Paffenroth, R.C., Champneys, A.R., Fairgrieve, T.F., Kuznetsov, Y.A., Oldeman, B.E., Sandstede, B., Doedel, E.J., Wang, X.: AUTO 2000: Continuation and bifurcation software for ordinary differential equations. Available online at: http://sourceforge.net/project/showfiles.php?group_id = 21781, (2002)
12. Rand, R.H.: Lecture Notes in Nonlinear Vibrations (version 45). Internet-First University Press, Ithaca, NY. Available online at: http://dspace.library.cornell.edu/handle/1813/79 (2004)